https://dx.doi.org/10.22161/ijaers.75.7 *ISSN: 2349-6495(P) | 2456-1908(O)*

Dynamic decoupling in reinforced concrete columns in structural core shape and applied to bridges

Weslley Imperiano Gomes de Melo[1], Normando Perazzo Barbosa[2]

[1]Civil Engineering Undergraduate Course Professor, Federal Rural University of Pernambuco, Recife-PE, Brazil
ORCID: https://orcid.org/0000-0001-5750-3272
[2]Full Professor, Federal University of Paraiba, João Pessoa-PB, Brazil
ORCID : https://orcid.org/0000-0003-4497-8900

Abstract*—Bridges that are designed to transpose large valleys generally show low stiffness to the lateral bending and, therefore, it is not convenient to use the static modeling of the wind actuation. In this context, due to the large volume of concrete required for the molding of the pillars, it is fitting to design them with a cross section composed of thin walls, in order to confer economy, and with one of the faces open and braced by lintels to guarantee greater stiffness to the deformation by bending due to the performance of the shear forces. Such dynamic modeling of the pillars activates bending-torsion and presents stiffness to the structure bending divided into two matrices: [J] and [S]. Due to the structural stiffness not being bonded in a single matrix, Rayleigh´s proportionality in the damping matrix assembly [C] does not apply. Thus, the formulation for such an assembly of [C] is proposed in this paper via the first three vibration modes of the structure. It models, with examples of application, a bridge with a deck backed on three pillars shaped as structural core braced by lintels and of thin-walled sections. Such pillars, with axes referenced in the torsional center of each, are inclined of β in relation to the global referential of the bridge coordinates, in order to apply the decoupling process of the differential equation system that governs the phenomenon and the resulting referential transformations. The vibration modes are verified by modeling with the ANSYS 2019 R1 software academic version.*

Keywords*—*Dynamic decoupling, Bridge pillars, Wall panels, Proportional damping, Bending-Torsion.

I. INTRODUCTION

In the dynamic analysis of the usual structures, it is convenient to model the stiffness of the elements that compose them and group them into the unique stiffness matrix [*K*] of the structure in the global coordinate reference. As for the pseudo-force due to the inertia that the structure exhibits when moving during the dynamic load, it is computed in the product of the mass matrix [*M*] by the acceleration vector of the linear and angular displacements $\{\ddot{D}\}$. Finally, the viscous damping of the structure is modeled by a damping matrix [*C*] proportional to the others, where such proportionality is determined by modal analysis and the resulting first two vibration modes. Thus, it is carried out following the example of Blume [1], and Fleming and Romualdi [2].

On the other hand, the analysis of the pillar with cross section composed of thin walls results in two stiffness matrices. The first [*J*] refers to the portion of the bending stiffness resulting from the pillar itself, and the second [*S*] relates to the bending stiffness of the lintels that promote the pillar bracing along the height at the open end of the cross section. When highlighting the equation of the mentioned Wall Panels, Smith and Taranath [3] and also Stamato and Mancini [4] are mentioned. In such analyses, the static imposition of the loading is done. However, in the dynamic analysis, which will be carried out here, the inertial pseudo-force portion is added to the motion, and so the Partial Differential Equations system (PDE's) is constituted by three matrices and, to that end, the proportionality procedure for the assembly of the damping matrix [*C*] of the thin wall pillars is proposed. For such a proposition, the decoupling of the PDE system based on Rosman [5] and necessary transformations of referential via Glück [6] are used. Finally, the wind effect is adopted as a function of two variables $q(x, t)$, in terms of the height x of the bridge pillar and under variation over time $g(t)$. To that end, the positioning of the center of mass is needed for such

https://dx.doi.org/10.22161/ijaers.75.7 *ISSN: 2349-6495(P) | 2456-1908(O)*

equation, as inspired by Hart [7], Vaicaitis [8], Laier [9] and Awruch [10].

The modeling of the wind action in the structures is processed, in the majority, from the perspective of the imposition of static loads. However, for the case of high-section thin-walled pillars (in works of art), lateral rigidity is reduced, making dynamic analysis of such a request important. This article proposes the systematization of the dynamic analysis of such requests in the pillars, thus providing a tool for manual calculation or even a mechanism of verification of the results obtained by modeling by commercial software.

II. THE WALL PANEL THEORY

The bridge pillar, considered of cross section made of thin and open walls, is conveniently analyzed through the Wall Panel Theory. Such technique consists of subdividing the core-shaped pillar into several walls and equating the balance of forces and moments for the internal forces and compatibilizing loads at the intersections of said walls. Finally, the differential equations of deflections and deformations are used. See Figure 1.

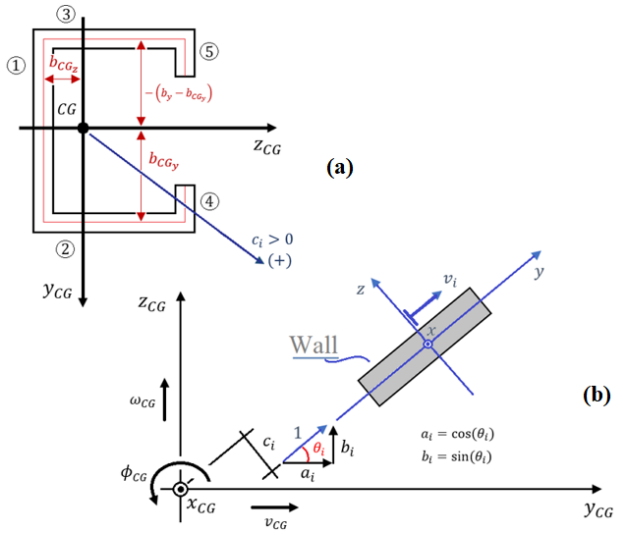

Fig. 1: Wall panels: (a) Drawing dimension notations, (b) Wall referential transformation

Such equation results in Ordinary Differential Equations (ODEs) in terms of the rotation v', third derivative from the displacements v, and the shear forces $\{V_f\}$ generated by external loads. The referred equations are written in terms of the center of gravity (*CG*) referential as:

$$-[J].\{v'''_{CG}\} + [S].\{v'_{CG}\} = \{V_f\} \quad (1)$$

where: $[J]$ - Bending stiffness matrix of the Wall Panels; $[S]$ - Lintel bending stiffness matrix; $\{v_{CG}\}$ - Vector of linear displacements: v (towards y), ω (towards z) and angularsφ (rotation around axial axis x); $\{V_f\}$- Vector of shear forces generated by external loading. The matrices $[J]$ and $[S]$, as well as the vector $\{V_f\}$ are found in Melo [11].

III. DYNAMIC FORMULATION

The static analysis of the Wall Panels, presented in equation (1), is expressed with reference in the center of gravity (*CG*). However, in the dynamic analysis, the inertial pseudo-force plot $[M].\{\ddot{v}\}$ is, in terms of mass, distributed m at the height H of the pillar, with reference in the center of mass (*CM*). In addition, the mass distribution modeling under acceleration $\ddot{z}$ is shown in Figure 2.

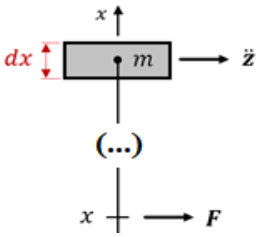

Fig. 2: Distributed mass subject to acceleration z̈

The aforementioned pseudo-force is expressed as:

$$F = \int_x^H (m.\ddot{z})\, dx \quad (2\,a)$$

$$m = \frac{M}{H} \quad (2\,b)$$

where: m – distributed mass; M – total column mass; H – column height.

For the tridimensional structure, there is:

$$\{dF\} = [M].\{\ddot{v}\} = \begin{bmatrix} m & 0 & 0 \\ 0 & m & 0 \\ 0 & 0 & I_p \end{bmatrix}.\begin{Bmatrix} \ddot{v} \\ \ddot{\omega} \\ \ddot{\phi} \end{Bmatrix} \quad (3)$$

where: I_p – Column inertia moment; $[M]$ – Mass matrix in the CM.

Because the dynamic plot expressed in equation 3 is referenced in the center of mass (*CM*) and the static plot in the center of gravity (*CG*), the coordinate transformation of the (*CM*) into the (*CG*) turns necessary. See Figure 3.

https://dx.doi.org/10.22161/ijaers.75.7 *ISSN: 2349-6495(P) | 2456-1908(O)*

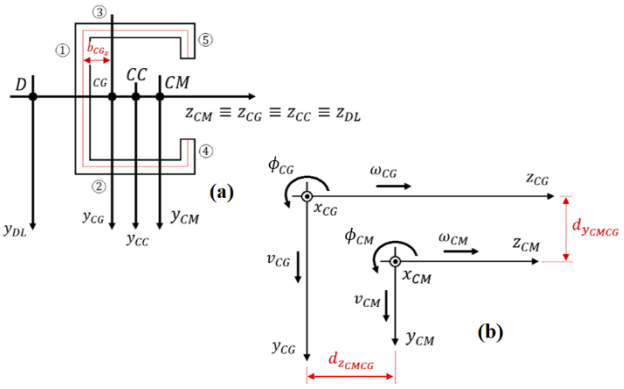

Fig. 3: Mass and gravity centers: (a) Positioning, (b) Referential transformation of the CM into CG

The relation of the displacements in the Center of mass to the detriment of the Center of gravity is worth:

$$v_{CM} = v_{CG} - d_{z_{CMCG}} . \phi_{CG} \quad (4\,a)$$

$$\omega_{CM} = \omega_{CG} + d_{y_{CMCG}} . \phi_{CG} \quad (4\,b)$$

$$\phi_{CM} = \phi_{CG} \quad (4\,c)$$

Matrically, the equations (4), expressed as law of coordinate transformation of the Center of Mass into the Center of Gravity, are expressed as:

$$\{v_{CM}\} = [\bar{T}_M].\{v_{CG}\}$$

$$\therefore \quad \begin{Bmatrix} v_{CM} \\ \omega_{CM} \\ \phi_{CM} \end{Bmatrix} = \begin{bmatrix} 1 & 0 & -d_{z_{CMCG}} \\ 0 & 1 & d_{y_{CMCG}} \\ 0 & 0 & 1 \end{bmatrix} . \begin{Bmatrix} v_{CG} \\ \omega_{CG} \\ \phi_{CG} \end{Bmatrix} \quad (5)$$

where: $\{v_{CM}\}$ – Vector of displacements in the Center of mass; $\{v_{CG}\}$ – Vector of displacemtns in the center of gravity; $[\bar{T}_M]$ – Matrix of linear transformation from *CM* into *CG*.

Resulting from the transformation Law expressed in equation (5), the Wall Panel movement plot of equation (3) is rewritten as:

$$\{dF_{CM}\} = [M].\{\ddot{v}_{CM}\} = [\bar{T}_M]^T.[M].[\bar{T}_M].\{\ddot{v}_{CG}\} \quad (6)$$

Deriving equation (1) and adding equation (6), results in the ODE´s system that governs the dynamic problem of the Wall Panels, expressed by:

$$-[J].\{v''''_{CG}\} + [S].\{v''_{CG}\} + [\bar{M}].\{\ddot{v}_{CG}\} = \{V'_f\} \quad (7)$$

where: $[\bar{M}] = [\bar{T}_M]^T.[M].[\bar{T}_M]$, $[\bar{M}]$ – Matrix of referenced mass in the *CG*, and: $V'_{ext} = 2.D_1.x + D_2$; $D_2 = -q_1$; $D_1 = -\frac{q_2}{2.H}$; $\{V'_f\} = V'_{ext}.\{A^*\}$; $V_{ext} = D_1.x^2 + D_2.x + D_3$; $D_3 = Q + q_1.H$.

IV. DYNAMIC DECOUPLING

The first procedure is to rewrite the system of ODEs (equation 7) in the main frame of the bending pillar stiffness $[]^*$ by linear transformation by rotation matrix [Re]. Then, $[]^*$ is transformed into $[]^{**}$ which is equivalent to the matrix Identity [I] via pre-multiplication and multiplication by $[]^{*-1/2}$ in order to maintain the symmetry of the other matrices and guarantee subsequent modal orthogonality and be able to use transposed matrices instead of inverse matrices. Finally, $[M^{**}]$ and $[S^{**}]$ are diagonalized through an iterative process until all terms outside the main diagonals of the matrices become of inferior module at a determined tolerance ε. The set of decoupled PDE´s in the generalized referential, for the nondamped Wall Panels is expressed as:

$$-q''''_j(x,t) + s_j.q''_j(x,t) + m_j.\ddot{q}_j(x,t) = V^0_{f_j}(x,t) \quad (8)$$

where: s_j is the j-th element of the main diagonal of the stiffness matrix of the diagonalized lintel bending [s]; m_j is the j-th element for the diagonalized mass matrix [m]; and j is the j-th vibration mode of the structure.

In the second procedure, the term of the damping $[C].\{\dot{v}''''\}$ is added with the damping matrix [*C*] constituted in terms proportional to the other matrices. Thus, the PDE system of viscously damped vibration for the Wall Panels is expressed by:

$$[\bar{M}].\{\ddot{v}_{CG}\} + [C].\{\dot{v}''''_{CG}\} + [S].\{v''_{CG}\} - [J].\{v''''_{CG}\} = \{V'_f\} \quad (9)$$

where: $[C] = \alpha_M.[\bar{M}] + \alpha_S.[S] - \alpha_J.[J]$, $[C]$ – Viscous damping matrix.

In the present decoupling, three referential transformations are made, where: the first transformation consists of diagonalizing the mass matrix $[\bar{M}]$ referenced in the *CG* by means of diagonalization routine (for example the Jacobi Method); in the second transformation, $[m^*]$ becomes the identity matrix [*I*] by pre-multiplication and multiplication by $[m^*]^{-1/2}$; and finally, in the third transformation, a looping process is applied for the joint diagonalization of $[S^{**}]$ and $[J^{**}]$ up to a certain tolerance adopted ε_S and ε_J. See Flow Chart shown in Figure 4.

And resulting as a set of decoupled PDE´s, expressed as:

$$\ddot{q}_j(x,t) + c_j.\dot{q}''''_j(x,t) + s_j.q''_j(x,t) - j_j.q''''_j(x,t) = V^0_{f_j}(x,t) \quad (10)$$

https://dx.doi.org/10.22161/ijaers.75.7 *ISSN: 2349-6495(P) | 2456-1908(O)*

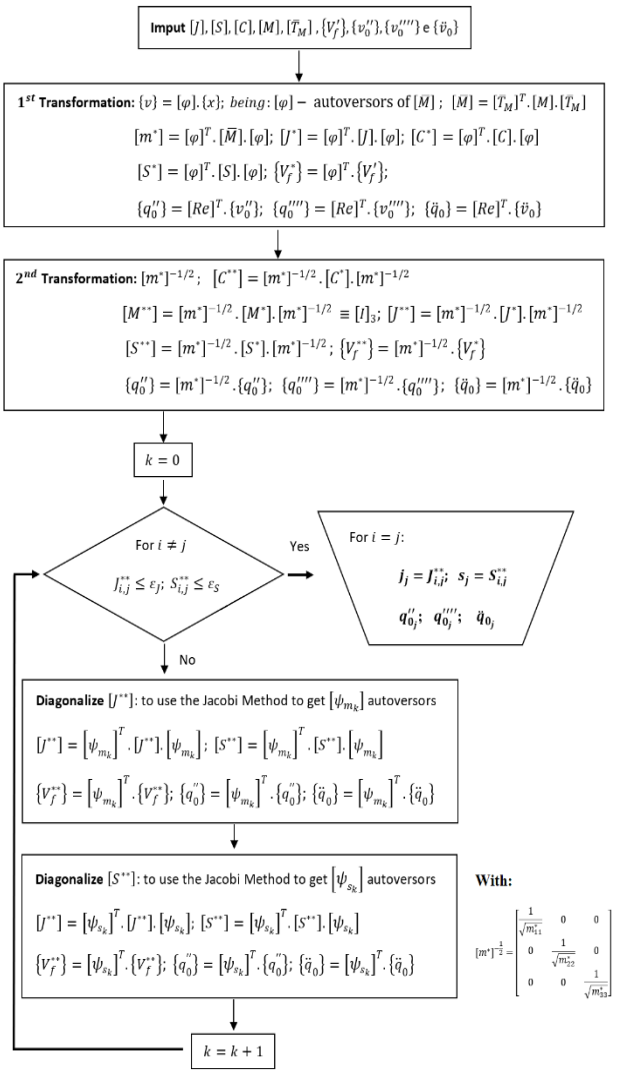

Fig. 4: Dynamic decoupling flowchart via Procedure 2

V. MODAL ANALYSIS

The ODE is written in the space x and temporal in t by means of the PDE´s resolution by the Method of Modal Superposition for the nondamped vibration as:

$$j_j.u''''(x) - s_j.u''(x) - \omega_j^2.u(x) = 0 \qquad (11\ a)$$

$$\ddot{g}(t) - \omega_j^2.g(t) = 0 \qquad (11\ b)$$

where: $q(x,t) = u(x).g(t)$, ω_j is the j-th vibration frequency of the structure.

The analysis of equation 11 (a) is carried out in order to determine the vibration modes and correlate s_j and j_j. Then, $u(x) = e^{\alpha.x}$ is applied and the characteristic equation is expressed by:

$$j_j.\alpha^4 - s_j.\alpha^2 - \omega_j^2 = 0 \qquad (12)$$

Where the roots of the characteristic equation, equation (12), α_1 and α_2, and the relation j_j and s_j in terms of the j-th vibration frequency of the structure expressed by:

$$\alpha_1 = \sqrt{\sqrt{\left(\frac{s_j}{2.j_j}\right)^2 + \frac{\omega_j^2}{j_j}} + \frac{s_j}{2.j_j}} \qquad (13\ a)$$

$$\alpha_2 = \sqrt{\sqrt{\left(\frac{s_j}{2.j_j}\right)^2 + \frac{\omega_j^2}{j_j}} - \frac{s_j}{2.j_j}} \qquad (13\ b)$$

$$j_j = \frac{s_j.\alpha^2 + \omega_j^2}{\alpha^4} \qquad (13\ c)$$

The solution of the displacements $u(x)$ is expressed as:

$$u(x) = C_1.sinh(\alpha_1.x) + C_2.cosh(\alpha_1.x) + C_3.sin(\alpha_2.x) + C_4.cos(\alpha_2.x) \qquad (14)$$

Adopting the nondimensionalization of the roots α into λ, via $\lambda_1 = \alpha_1.H$ and $\lambda_2 = \alpha_2.H$, roots λ_1 and λ_2 are correlated by:

$$\lambda_1^2 - \lambda_2^2 = \lambda^2 \qquad (15\ a)$$

$$\lambda = H.\sqrt{\frac{s_j}{j_j}} \qquad (15\ b)$$

Also, by applying the nondimensionalized roots α_1 and α_2 in the form of λ_1 and λ_2 and multiplying the latter, the frequencies of the structure are expressed as:

$$\omega_j = \omega_j^*.\frac{\sqrt{j_j}}{H^2} \qquad (16\ a)$$

$$\omega_j^* = \lambda_1.\lambda_2 \qquad (16\ b)$$

The pillar analyzed here is of the fixed-in-the-base type, therefore, with displacement u (x = 0) = 0 null and rotation $u'(x=0) = 0$ also null. At the top, the end is free and, at a subsequent moment, bending and stress are shear and null, thus applying: $u''(x=H) = u'''(x=H) = 0$, respectively. Applying such boundary conditions in equation (14), after due nondimensionalization, the linear equation system results in:

$$\begin{bmatrix} 1 & 0 & 1 & 0 \\ 0 & \lambda_1 & 0 & \lambda_2 \\ \lambda_1^2.cosh(\lambda_1) & \lambda_1^2.sinh(\lambda_1) & -\lambda_2^2.cos(\lambda_2) & -\lambda_2^2.sin(\lambda_2) \\ \lambda_1^3.sinh(\lambda_1) & \lambda_1^3.cosh(\lambda_1) & \lambda_2^3.sin(\lambda_2) & -\lambda_2^3.cos(\lambda_2) \end{bmatrix} \cdot \begin{Bmatrix} C_1 \\ C_2 \\ C_3 \\ C_4 \end{Bmatrix} = \{0\} \qquad (17)$$

The nontrivial solution of the system, shown in equation (17), leads to the transcendental equation:

$$f_1.cosh(\lambda_1).cos(\lambda_2) + f_2.sinh(\lambda_1).sin(\lambda_2) = -1 \qquad (18)$$

https://dx.doi.org/10.22161/ijaers.75.7 *ISSN: 2349-6495(P) | 2456-1908(O)*

with: $f_1 = \dfrac{2.\lambda_1^3.\lambda_2^3}{\lambda_1.\lambda_2^5 + \lambda_1^5.\lambda_2}$, $f_2 = \dfrac{\lambda_1^2.\lambda_2^4 - \lambda_1^4.\lambda_2^2}{\lambda_1.\lambda_2^5 + \lambda_1^5.\lambda_2}$.

Highlighting that, the period will be:

$$T_j = \frac{2.\pi}{\omega_j} = T_j^*.\frac{H^2}{\sqrt{j_j}} \qquad (19\ a)$$

$$T_j^* = \frac{2.\pi}{\lambda_1.\lambda_2} \qquad (19\ b)$$

In Figure 5, the change in the elastic line in the first four vibration modes is presented for $\lambda^2 = 0$. Figure 6 shows the ANSYS modeling, evidencing some vibration modes of the column with open cross section and thin walls.

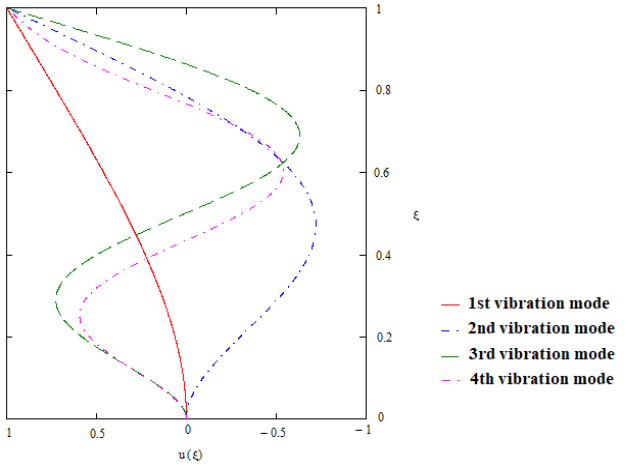

Fig. 5: The first four vibration modes of the Pillar m with fixed-at-the-base core

Now, through the relation between the nondimensionalized roots λ_1 and λ_2, constant in equation 15 (a), and in the substitution of the harmonic and hyperbolic terms for the Taylor Series with 11 terms, the vibration modes j = 1 to 7 are expressed by $\lambda = 0$, see Table 1.

Table. 1: Vibration modes of the Core Column by $\lambda^2 = 0$

	Mode $i=1$	Mode $i=2$	Mode $i=3$	Mode $i=4$	Mode $i=5$	Mode $i=6$	Mode $i=7$
λ_1	1.87510	4.69409	7.85483	9.08911	10.02092	11.68901	14.62618
λ_2	1.87510	4.69409	7.85483	9.08911	10.02092	11.68901	14.62618
ω_i^*	3.51600	22.03448	61.69835	84.61192	105.97714	136.63295	213.92514
T_i^*	1.78703	0.28515	0.10184	0.07606	0.05929	0.04599	0.02937

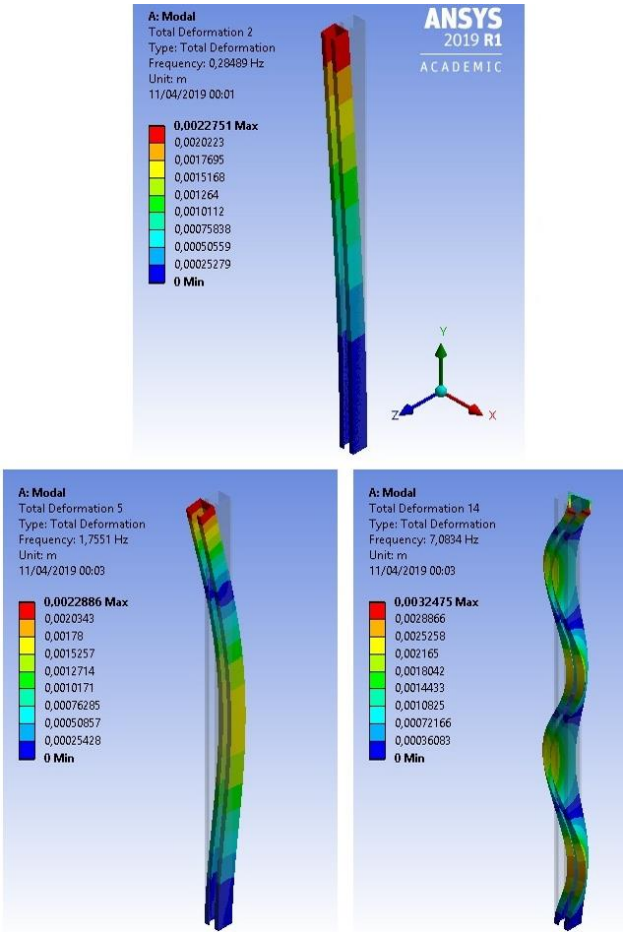

Fig. 6: Vibration modes by modeling with the ANSYS 2019 R1 software academic version

VI. PROPORTIONAL DAMPING

Procedure 2 of diagonalization of the PDE´s system presented in equation(9) results in:

$$c_j = \alpha_M.1 + \alpha_S.s_j - \alpha_J.j_j \qquad (20)$$

The analysis of the PDE shown in equation (10) and subsequent application of $u(x) = e^{\alpha x}$ and $g(t) = e^{\omega t}$, results as a characteristic equation of the damped free vibration:

$$\omega^2 + \left(c_j.\alpha^4\right).\omega + \left(s_j.\alpha^2 - j_j.\alpha^4\right) = 0 \qquad (21)$$

The resolution of the characteristic equation, equation (21), with the imposition of critical damping and subsequent u of the damping ratio ξ_j implies c_j^0 equals to:

$$c_j^0 = 2.\xi_j.\omega_j \qquad (22)$$

where: ξ_j – damping ratio of the $^{J\text{-th}}$ vibration mode.

Equations 13 (c) and 15 (b) with due nondimensionalization of the roots $\lambda_1 = \alpha_1.H$ and $\lambda_2 = \alpha_2.H$, result in s_j and j_j in terms of the frequency ω_j, as:

https://dx.doi.org/10.22161/ijaers.75.7 *ISSN: 2349-6495(P) | 2456-1908(O)*

$$j_j = \frac{\omega_j^2}{(\lambda_1^4 - \lambda_1^2.\lambda^2)} \quad (23\ a)$$

$$s_j = \lambda^2.j_j \quad (23\ b)$$

Finally, since it is only desired to establish proportions of the matrices $[\bar{M}]$, $[J]$ and $[S]$ that form the damping matrix $[C]$, the application of equations (22) and (23) in the condition expressed in equation (20) and using the frequency ω_j^* instead of ω_j, since it is only desired to establish proportions of the matrices results in :

$$\xi_j = \frac{\alpha_M}{2.\omega_j^*} + \frac{\alpha_S.s_j}{2.\omega_j^*} - \frac{\alpha_J.j_j}{2.\omega_j^*} \quad (24)$$

Imposing the first three vibration modes $j = 1, 2$ and 3 in equation (24), a system of equations is built, whose solution is:

$$\alpha_M = \frac{2.[\omega_1^*.\xi_1(j_2.s_3 - j_3.s_2) + \omega_2^*.\xi_2(j_3.s_1 - j_1.s_3) + \omega_3^*.\xi_3(j_1.s_2 - j_2.s_1)]}{j_1.(s_2 - s_3) + j_2.(s_3 - s_1) + j_3.(s_1 - s_2)} \quad (25\ a)$$

$$\alpha_S = \frac{2.[\omega_1^*.\xi_1(j_3 - j_2) + \omega_2^*.\xi_2(j_1 - j_3) + \omega_3^*.\xi_3(j_2 - j_1)]}{j_1.(s_2 - s_3) + j_2.(s_3 - s_1) + j_3.(s_1 - s_2)} \quad (25\ b)$$

$$\alpha_J = \frac{2.[\omega_1^*.\xi_1(s_3 - s_2) + \omega_2^*.\xi_2(s_1 - s_3) + \omega_3^*.\xi_3(s_2 - s_1)]}{j_1.(s_2 - s_3) + j_2.(s_3 - s_1) + j_3.(s_1 - s_2)} \quad (25\ c)$$

In percentual terms there are:

$$\mu_M = \frac{\alpha_M}{\alpha_M + \alpha_S + \alpha_J} \quad (26\ a)$$

$$\mu_S = \frac{\alpha_S}{\alpha_M + \alpha_S + \alpha_J} \quad (26\ b)$$

$$\mu_J = \frac{\alpha_J}{\alpha_M + \alpha_S + \alpha_J} \quad (26\ c)$$

a) Center of Mass Positioning

For the reinforced concrete, cross, and thin-walled open section, the determination of the center of mass coordinates (*CM*) is made necessary. To this end, the following definitions are used:

$$x_{CM}^* = \frac{\sum_{i=1}^n x_{CM_i}^*.m_i}{\sum_{i=1}^n m_i} \quad (27\ a)$$

$$y_{CM}^* = \frac{\sum_{i=1}^n y_{CM_i}^*.m_i}{\sum_{i=1}^n m_i} \quad (27\ b)$$

where: $x_{CM_i}^*$ and $y_{CM_i}^*$ – coordinates of the canonic center of mass i in relation to a generic referential x^* and y^* defined in the cross section; m_i – canonic element mass i;n – number of canonic masses that formed in core; and x_{CM}^* and y_{CM}^* – the center of mass coordinates of the cross section in core shape in relation to referential x^* and y^*.

The adoption of the subdivision presents in Figure 7, the concrete specific mass $\rho_{CS} = 2400\ kg/m$ steel $\rho_S = 7860\ kg/m^3$ results in:

$$x_{CM}^* = \frac{x_{CM_1}^*.m_1 - x_{CM_2}^*.m_2 - x_{CM_3}^*.m_3 - x_{CM_4}^*.M_4 + x_{CM_5}^*.M_5}{m_1 - m_2 - m_3 - M_4 + M_5} \quad (28\ a)$$

$$y_{CM}^* = \frac{y_{CM_1}^*.m_1 - y_{CM_2}^*.m_2 - y_{CM_3}^*.m_3 - y_{CM_4}^*.M_4 + y_{CM_5}^*.M_5}{m_1 - m_2 - m_3 - M_4 + M_5} \quad (28\ b)$$

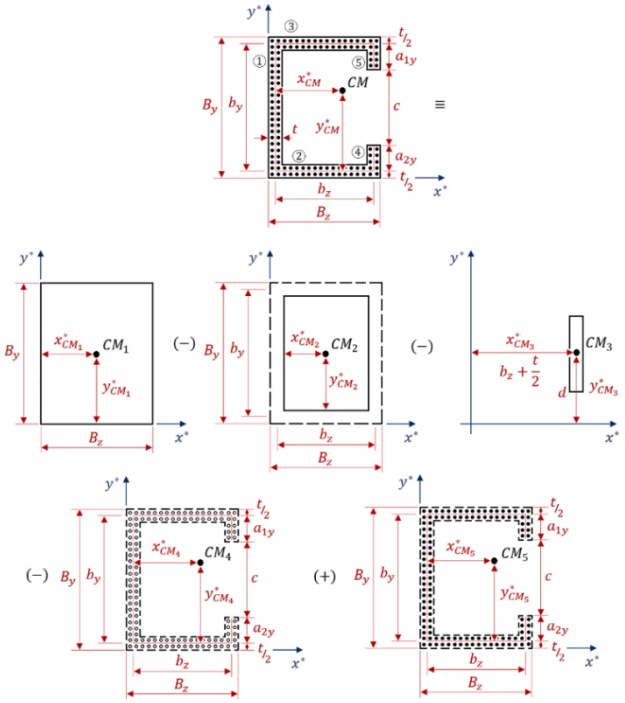

Fig. 7: Geometry of decomposition into canonic format masses

Finally, the distances between the centers of mass (*CM*) and that of gravity (*CG*) are valid, according to what is shown in Figure8:

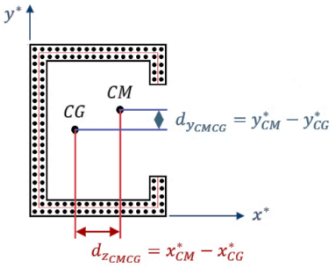

Fig. 8: Positioning of the CG and CM in the cross section

$$d_{y_{CMCG}} = y_{CM}^* - y_{CG}^* \quad (29\ a)$$

$$d_{z_{CMCG}} = x_{CM}^* - x_{CG}^* \quad (29\ b)$$

https://dx.doi.org/10.22161/ijaers.75.7 *ISSN: 2349-6495(P) | 2456-1908(O)*

VII. REFERENTIAL TRANSFORMATION

a) Transfer from the center of gravity CG to the torsional center D

According to the compatibilization of the rotations ϕ_D (in the torsional center) and ϕ_{CG} (in the center of gravity), the displacements $\omega_D$via ω_{CG}, and projection of the distance $d_{y_{CGD}}$ from the center of gravity to the torsional center parallel to z axis, procedures are the same forv_D with v_{CG} and $d_{z_{CGD}}$. See Figure9.

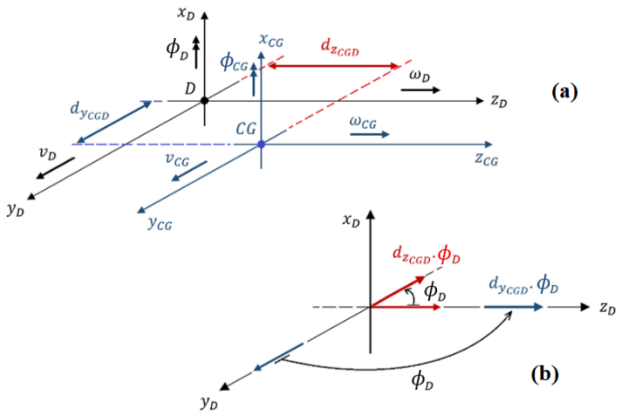

Fig. 9: Transformation of the referential in the CG for D: (a) translation, (b) rotation

The matricial format of the displacement balance is:

$$\{v_{CG}\} = [\bar{T}_D].\{v_D\} \quad (30\ a)$$

$$\begin{Bmatrix} v_{CG} \\ \omega_{CG} \\ \phi_{CG} \end{Bmatrix} = \begin{bmatrix} 1 & 0 & -d_{z_{CGD}} \\ 0 & 1 & d_{y_{CGD}} \\ 0 & 0 & 1 \end{bmatrix} . \begin{Bmatrix} v_D \\ \omega_D \\ \phi_D \end{Bmatrix} \quad (30\ b)$$

b) Transfer from the torsional center D for the source of the coordinates 0_s

Analogously as in (a) of this item, and considering the rotation β between the referential (y_{DL}, z_{DL}, x_{DL}) in the torsional center and the global referential (y_g, z_g, x_g), see Figure 10, there is:

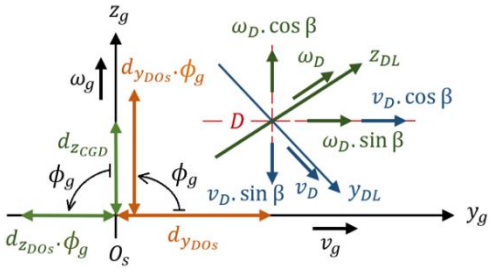

Fig. 10: Transformation of the referential in the torsional center D for the source O_s.

$$v_D.cos\beta + \omega_D.sin\beta = v_g - d_{z_{DO_s}}.\phi_g \quad (31\ a)$$

$$-v_D.sin\beta + \omega_D.cos\beta = \omega_g + d_{y_{DO_s}}.\phi_g \quad (31\ b)$$

$$\phi_D = \phi_g \quad (31\ c)$$

Matrically, the balance is expressed as:

$$\{v_D\} = [\bar{T}_S]^{-1}.[\bar{T}_G].\{v_g\} \quad (32\ a)$$

$$\begin{Bmatrix} v_D \\ \omega_D \\ \phi_D \end{Bmatrix} = \begin{bmatrix} cos\beta & sin\beta & 0 \\ -sin\beta & cos\beta & 0 \\ 0 & 0 & 1 \end{bmatrix}^{-1} . \begin{bmatrix} 1 & 0 & -d_{z_{DO_s}} \\ 0 & 1 & d_{y_{DO_s}} \\ 0 & 0 & 1 \end{bmatrix} . \begin{Bmatrix} v_g \\ \omega_g \\ \phi_g \end{Bmatrix} \quad (32\ b)$$

Combining equations (30) and (32), direct transfer from *CG* to O_s is as follows:

$$\{v_g\} = [\bar{T}_S]^{-1}.[\bar{T}_G].[\bar{T}_D]^{-1}.\{v_{CG}\} \quad (33)$$

VIII. RESULTS AND DISCUSSIONS

In this section, a bridge with a deck backed over three pillars, each with a cross section composed of thin walls will be analyzed. See Figure 11.All in compliance with the Technical Standards NBR 7188 [12] and DIN 1055 [13].

The material used is reinforced concrete of resistance class C – 40, complying with NBR 6118 [14]. Therefore, the modules are of longitudinal elasticity $E = 3.54175\ x\ 10^7\ kN/m^2$ and of cross elasticity $G = 1.47573\ x\ 10^7\ kN/m^2$, as well as Poisson's coefficient $v = 0.20$. On the basis of the loading conditions of the bridge, two scenarios are analyzed: in the first scenario, the sole actuation of the wind on the structure (See Example 1) and, in the second scenario, the traffic performance with a focus on braking (See Example 2).

EXAMPLE 1: In this first analysis, the bridge is subject to the sole actuation of the lateral wind in the form of three loadings along the height of the pillar, namely: $q_1 = 20\ kN/m$, $q_2 = 30\ kN/m$ and $Q = 10\ kN$. See Figure 12.

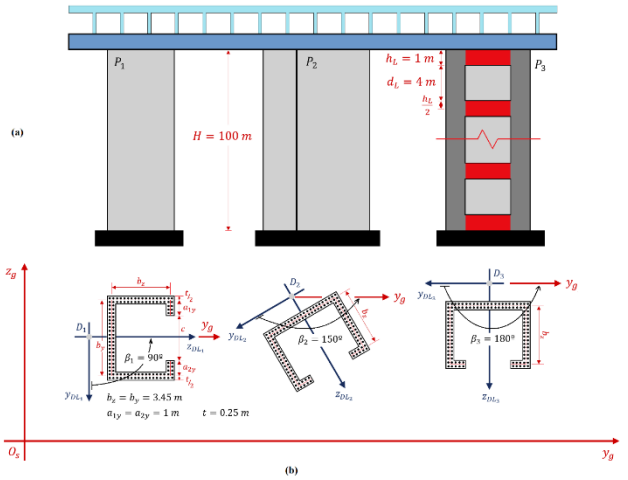

Fig. 11: Bridge backed over three thin-walled pillars: (a) lateral view, (b) drawing configuration of the pillars

https://dx.doi.org/10.22161/ijaers.75.7 *ISSN: 2349-6495(P) | 2456-1908(O)*

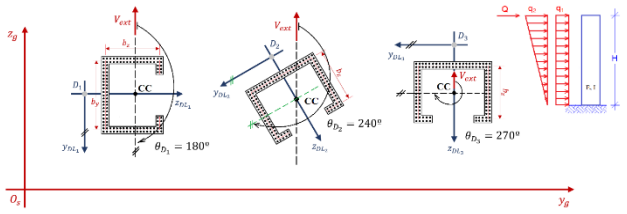

Fig. 12: Angles formed between the external shear forces$V_{ext_{P_1}}, V_{ext_{P_2}}, V_{ext_{P_3}}$ and axes y_{DL} defined in the torsional centers of each of the three columns

$$V_{ext_y} = -\frac{q_{2y}}{2.H}.x^2 - q_{1y}.x + \left(Q_y + q_{1y}.H\right)$$

$$q_{1y} = q_1.\cos(\theta_D)\,;\ q_{2y} = q_2.\cos(\theta_D)\,;\ Q_y = Q.\cos(\theta_D)$$

$$q_{1z} = q_1.\sin(\theta_D)\,;\ q_{2z} = q_2.\sin(\theta_D)\,;\ Q_z = Q.\sin(\theta_D)$$

$$V_{ext_z} = -\frac{q_{2z}}{2.H}.x^2 - q_{1z}.x + (Q_z + q_{1z}.H)$$

The shear force, over time, will be governed by a harmonic sinusoidal function $V_g(t) = sin(\bar{\omega}.t)$, with frequency $\bar{\omega} = 3\,rad/s$. In addition, the PDE system of equation (9) is expressed for the pillars and referenced in the center of gravity as:

$$\begin{bmatrix} 7870.65 & 0 & 387.78 \\ 0 & 7870.65 & 1506.08 \\ 387.78 & 1506.08 & 319.73 \end{bmatrix}.\begin{Bmatrix} \ddot{v} \\ \ddot{\omega} \\ \ddot{\phi} \end{Bmatrix} + \begin{bmatrix} 120073 & 0 & -18909 \\ 0 & 99853 & 5459 \\ -22378 & 0 & 174899 \end{bmatrix}.\begin{Bmatrix} \dot{v}'''' \\ \dot{\omega}'''' \\ \dot{\phi}'''' \end{Bmatrix} + \begin{bmatrix} 0 & 0 & 6939 \\ 0 & 0 & 10919 \\ 0 & 0 & -12427 \end{bmatrix}.\begin{Bmatrix} v'' \\ \omega'' \\ \phi'' \end{Bmatrix} - \begin{bmatrix} 240146 & 0 & -44757 \\ 0 & 199706 & 0 \\ -44757 & 0 & 336224 \end{bmatrix}.\begin{Bmatrix} v'''' \\ \omega'''' \\ \phi'''' \end{Bmatrix} = \{V_f\}$$

The same PDE system, with the proportionality coefficients of the matrices $[\bar{M}]$, $[J]$ and $[S]$ to compose the viscous damping matrix $[C]$, is expressed as: $\alpha_M = 0;\ \alpha_S = -3.80\,x\,10^{16};\ \alpha_J = -3.80\,x\,10^{16};\ \mu_M = 0;\ \mu_S = 0.5;\ \mu_J = 0.5.$

And the set of decoupled PDE´s presented in equation (10) are:

$$-q_1''''(x,t) + 0.03385.\ddot{q}_1(x,t) + 0.49519.\dot{q}_1''''(x,t) - 0.00962.q_1''(x,t) = V_{f_1}^0(x,t)$$

$$-q_2''''(x,t) + 0.04038.\ddot{q}_2(x,t) - 0.13363.\dot{q}_2''''(x,t) - 1.26726.q_2''(x,t) = V_{f_2}^0(x,t)$$

$$-q_3''''(x,t) + 0.00003.\ddot{q}_3(x,t) + 0.50243.\dot{q}_3''''(x,t) + 0.00498.q_3''(x,t) = V_{f_3}^0(x,t) \quad (34)$$

In the set of EDP's presented in equations (34), the first mode of vibration (mobilizing the lintels) is verified by crossing the equation (15 b) and the Figure 13.

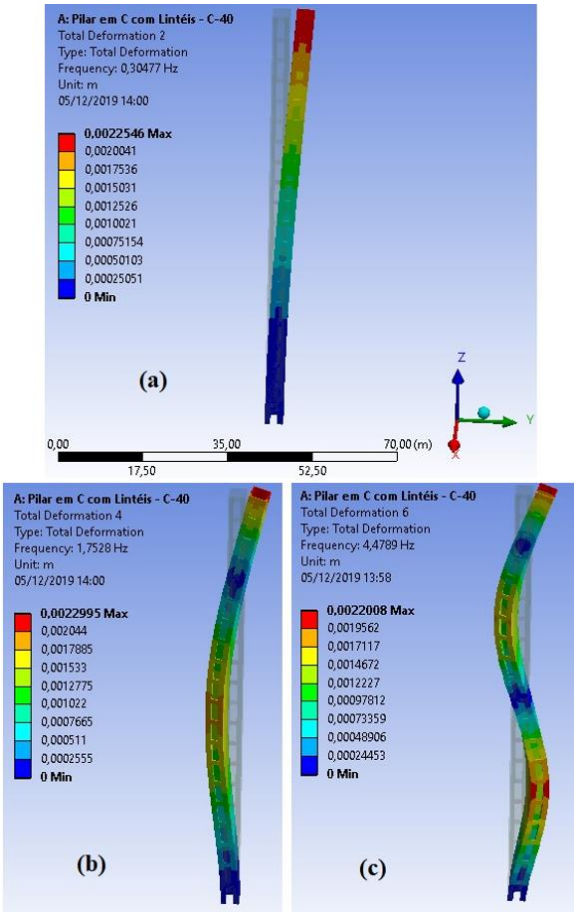

Fig. 13:Column C in concrete C - 40, vibration modes activating the lintels for flexion: (a) 1st mode ($\omega_1 = 1{,}91493\,rad/s$), (b) 2nd mode and (c) 3rd mode via modeling in ANSYS

so, with the parameters $s_j = -0{,}00962$ and $j_j = -1$, and through equation (15 b) the parameter is determined $\lambda = H.\sqrt{s_j/j_j} = 100\,[m].\sqrt{-0{,}00962/-1} = 9{,}81$, using Table 2 with the value immediately above λ, then: $\omega_1{}^* = 2{,}54634\,rad/s$ (for $\lambda = 10$).

Table. 2: Vibration modes of the Core Column by $\lambda = 10$

	Mode $i=1$	**Mode $i=2$**	**Mode $i=3$**	**Mode $i=4$**	**Mode $i=5$**	**Mode $i=6$**	**Mode $i=7$**
$\boldsymbol{\lambda_1}$	3,25746	5,50391	8,42839	9,64266	10,43138	11,87014	14,61565
$\boldsymbol{\lambda_2}$	0,78169	4,50478	7,81267	9,10938	9,94051	11,44116	14,26945
$\boldsymbol{\omega_i^*}$	2,54634	24,79389	65,84820	87,83870	103,69321	135,80821	208,55730
$\boldsymbol{T_i^*}$	2,46754	0,25342	0,09542	0,07153	0,06059	0,04627	0,03013

https://dx.doi.org/10.22161/ijaers.75.7 *ISSN: 2349-6495(P) | 2456-1908(O)*

Finally, in Figure 13 (a) the first vibration mode of a single C-shaped pillar and braced with lintels is presented under the same distribution as this example, hence the reason for comparison, with an approximation of 2.24 %.The frequency adjustment determined via TMC is used by the coefficient $\alpha = {}^{1}/_{1,3}$, whose functionality is based on Diziewolski [15].

$$\Delta(\%) = \frac{|\omega^*_{ANSYS} - \omega^*_{TMC}|}{\omega^*_{TMC}}.100\ \% = \\ = \frac{|1{,}91493 - 1{,}95872|\frac{rad}{s}}{1{,}95872\frac{rad}{s}}.100\ \% = 2{,}24\ \%$$

The shear force V_f functions in the initial referential are presented in Table 3, as well as V_f^0 in the generalized referential, and both for the columns P_1, P_2 and P_3.

Table. 3: Functions of the shear force per Column

	ColumnP_1	**ColumnP_2**	**ColumnP_3**
V_{f_1}	$89.77\,.x^2 + 11969.20\,.x - 1196926.12$	$-48.87\ .x^2 - 6515.63\,.x + 651565.87$	$-147.66\,.x^2 - 19687.64\,.x + 1968773.75$
V_{f_2}	$120.17\,.x^2 + 16023.05\,.x - 1602313.28$	$-141.82\,.x^2 - 18.908.90\,.x + 1809899.76$	$26.41\,.x^2 + 3520.92\,.x - 352093.65$
V_{f_3}	$332.19\,.x^2 + 44291.71\,.x - 4429193.40$	$-180.83\,.x^2 - 24110.90\,.x + 2411102.23$	$-546.40\,.x^2 - 72853.59\,.x + 7285395.07$
$V_{f_1}^0$	$0.18\,.x^2 + 24.43\,.x - 2442.55$	$-0.10\,.x^2 - 13.30\,.x + 1329.69$	$-0.30\,.x^2 - 40.17\,.x + 401750.64$
$V_{f_2}^0$	$0.27\,.x^2 + 35.85\,.x - 3585.47$	$-0.32\,.x^2 - 42.31\,.x + 4231.26$	$0.06\,.x^2 + 7.88\,.x - 787.97$
$V_{f_3}^0$	$0.59\,.x^2 + 78.21\,.x - 7820.51$	$-0.32\,.x^2 - 42.57\,.x + 4257.22$	$-0.96\,.x^2 - 128.64\,.x + 12863.63$

For the first vibration mode, the displacement function, $u(x)$ and $g(t)$, and the generalized and initial referential are, respectively:

$$u_1(x) = 0.36275\,.\{cosh(0.01983\,.x) - cos(0.01713\,.x) + 0.92535.[-\sinh(0.01983\,.x) + 2.41421.sin(0.01713\,.x)]\}$$

$$g_1(t) = 4.543\,.10^{10}.sin(3.476\,.10^{-3}.t) - 8.928\,.10^{8}.sin(3.t)$$

$$u_1(x) = 6.098\,.10^{-4}\,.\{cosh(1.847\,.10^{-3}\,.x) - cos(7.65\,.10^{-4}\,.x) + 1.556\,.10^{-3}.[-\sinh(1.847\,.10^{-3}\,.x) + 4.048\,.10^{-3}.sin(7.65\,.10^{-4}\,.x)]\}$$

$$g_1(t) = 7.637\,.10^{7}.sin(5.843\,.10^{-6}.t) - 1.501\,.10^{6}.sin(3.t)$$

Then, returning to the initial referential, the vector of displacements $\{v_{CG}\}$ for the mode of larger deformations is written as:

$$\{v_{CG}\}_1 = [\Phi_R].\{q\} = [\Phi_R].\{u_1(x).g_1(t)\}$$

where: $[\Phi_R] = [Re].[J^*]^{-\frac{1}{2}}.[\varphi_1].[\varphi_2].[\varphi_3].(\dots).[\varphi_{n-1}].[\varphi_n]$.

And, finally, the rotation function $\phi_{CG}(x)$ is expressed as:

$$\phi_{CG}(x) = u_1(x).g_1(t) + u_2(x).g_2(t) + u_3(x).g_3(t)$$

The relation between rotation $\phi_{CG}(x)$ and the Bimoment$B(x)$, originating from the Bending-Torsion Theory yields:

$$B(x) = E.I_\omega.\phi''_{CG}(x) = E.I_\omega.\frac{d^2[\phi_{CG}(x)]}{dx^2}$$

After applying the referential transformations, we have the Bimoment in the Base and in the Top for the *CG*, *D* and O_s. See Table 4, as well as the rotation in Table 5.

Table. 4: Bimoment values per Pillar in the CG and D, and the set of pillars in O_s

$(x\ 10^7)$ $kN.m^2$	**In the Center of Gravity**			**In the Torsional Center**			O_s
	CG_1	CG_2	CG_3	D_1	D_2	D_3	
$B(x=0)$	-3.99422	2.17432	6.56993	-3.99422	2.17432	6.56993	Idem per Pillar.
$B(x=50m)$	- 4.00790	2.18176	6.59242	- 4.00790	2.18176	6.59242	
$B(x=H)$	- 4.04993	2.20464	6.66156	- 4.04993	2.20464	6.66156	

Table. 5: Rotation values per Pillar in the CG and set of pillars in O_s

rad	**In the Center of Gravity**			O_s
	CG_1	CG_2	CG_3	
$\phi(x=0)$	0	0	0	Idem per Pillar.
$\phi(x=50m)$	- 57.42669	31.26114	94.45877	
$\phi(x=H)$	- 233.82458	127.28615	384.60827	

https://dx.doi.org/10.22161/ijaers.75.7 *ISSN: 2349-6495(P) | 2456-1908(O)*

EXAMPLE 2: In this second analysis, there is the braking force of the traffic and lateral cargo at the top. Thus, the shear force under the configuration shown in Figure 14 is presented as:

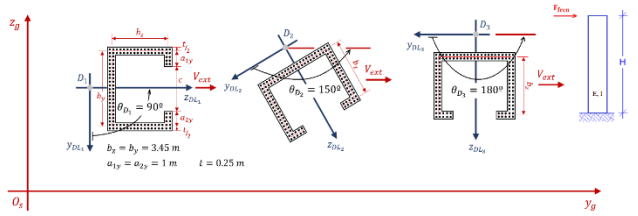

Fig. 14: Angles formed between the external shear forces activated by braking in each Pillar and the axes y_{DL} in each of the three columns

Adopting the same frequency $\bar{\omega} = 3\ rad/s$ for the shear force, the values of the Top and Base Bimoments are expressed in Table 6.

Tab. 6: Values of Bimoment for the actuation of the braking force of the vehicles

$(x\ 10^5)$ $kN.m^2$	In the Center of Gravity			In the Torsional Center			O_s
	CG_1	CG_2	CG_3	D_1	D_2	D_3	
$B(x=0)$	- 4.96373	2.70209	8.16464	- 4.96373	2.70209	8.16464	Idem per Pillar.
$B(x=50m)$	- 4.98075	2.71135	8.19264	- 4.98075	2.71135	8.19264	
$B(x=H)$	- 5.03302	2.73980	8.27860	- 5.03302	2.73980	8.27860	

where the loadings are: $q_1 = q_2 = 0\ kN/m$, $Q = 10\ kN$; the Top Bimoment $B_H = 10\ kN.m^2$; and the torsional moment at the top is null $M_{tH} = 0\ kN.m$.

IX. CONCLUSION

In this paper the implementation of the dynamic plots of acceleration and damping in the Wall Panel Theory was carried out, in order to promote the dynamic analysis of bridge pillars under the effect of Bending-Torsion and to provide the noncoincidence of the center of gravity with the torsional center, as a result of the geometry in thin-walled cross section. Moreover, the PDE system that governs the vibration of said Wall Panels has two bending stiffness matrices, being: [*J*] for the pillar itself and [*S*] for the lintels that promote bracing of said pillar. Thus, the Rayleigh proportional [C] damping matrix assembly considers only a single stiffness matrix. At this point, an unpublished formulation is made for such a composition. Two procedures of diagonalization of the PDE system and transformations between the reference points of the center of gravity (*CG*), the center of torsion (*D*) and a global origin (O_s) are discussed.

Such analyses encourage the of high columns in reinforced concrete subject of wind actuation, due to the large volume of concrete required for the molding of the pillars. It is fitting to design them with a cross section composed of thin walls, in order to confer economy, and with one of the faces open and braced by lintels.

REFERENCES

[1] Blume, J. A. (1968). Dynamic characteristics of multistory buildings. Journal of the structural division (ISSN: 0044-8001), 94(2), 377-402.

[2] Fleming, J. F. and Romualdi, J. P. (1961). Dynamic response of highway bridges. Journal of the structural division (ISSN: 0044-8001), 87(7), 31-61.

[3] Smith, B. S. and Taranath, B. S. (1972). The analysis of tall core-supported structures subject to torsion. Proceedings of civil engineering, 173-187.

[4] Stamato, M. C. and Mancini, E. (1973). Three-dimensional interaction of walls and frames. Journal of the structural division (ISSN: 0044-8001), 99(12), 2375-2390.

[5] Rosman, R. (1972). Application of variational methods in the theory of tall buildings structures. Proceedings of the international conference on variational methods in engineering, 11/68-11/83.

[6] Gluck, J. (1970). Lateral-load analysis of asymmetric multistory structures. Journal of the structural division (ISSN: 0044-8001), 96(2), 317-333.

[7] Hart, C. C. (1970). Building dynamics due to stochastic wind forces. Journal of the structural division (ISSN: 0044-8001), 96(3), 535-550.

[8] Vaicaitis, R. (1975). Response analysis of tall buildings. Journal of the structural division (ISSN: 0044-8001), 101(3), 585-600.

[9] Laier, J. E. (1984). Estudo do comportamento dinâmico de estruturas de edifícios altos pela Técnica do Meio Contínuo. Tese de Livre Docência. São Carlos: Universidade de São Paulo. In press.

[10] Awruch, A. M. (1993). Análisis de estructuras sujeitas a la acción del viento según la norma brasileira y conun enfoque estocástico. XXVI Jornadas Sudamericanas de ingenieria estructural (ISSN: 2316-2457), 3, 31-42.

[11] Melo, W. I. G. (2019). Contribuições à análise dinâmica da ação do vento em pilares de pontes via Técnica do Meio Contínuo e Método dos Elementos Finitos. Tese de Doutorado. João Pessoa: Universidade Federal da Paraíba. https://sig-arq.ufpb.br/arquivos/20200630605626186276475430 4487c5b/2019DO_WeslleyGomes_PDF_DEFINITIVO.pdf.

[12] ASSOCIAÇÃO BRASILEIRA DE NORMAS TÉCNICAS. NBR 7188. Rio de Janeiro: 2013.

[13] THE GERMAN INSTITUTE FOR STANDARDIZATION. DIN 1055. Anfor: 2005.

[14] ASSOCIAÇÃO BRASILEIRA DE NORMAS TÉCNICAS. NBR 6118. Rio de Janeiro: 2014.

https://dx.doi.org/10.22161/ijaers.75.7 *ISSN: 2349-6495(P) | 2456-1908(O)*

[15] Dziewolski, R. (1964). Étude théorique et experimentale d'une pouter en caisson asymétrique avec deux appendices. IABSE congress report, 7, 131-137.